6-6-2013

Methane Adsorption on Aggregates of Fullerenes: Site-Selective Storage Capacities and Adsorption Energies

Alexander Kaiser
University of Innsbruck

Samuel Zottl
University of Innsbruck

Peter Bartl
University of Innsbruck

Christian Leidlmair
University of Innsbruck

Andreas Mauracher
University of Innsbruck

See next page for additional authors

Recommended Citation

A. Kaiser, S. Zöttl, P. Bartl, C. Leidlmair, A. Mauracher, M. Probst, S. Denifl, O. Echt, and P. Scheier, Methane Adsorption on Aggregates of Fullerenes: Site-Selective Storage Capacities and Adsorption Energies, ChemSusChem 6 (2013) 1235 – 1244, DOI: 10.1002/cssc.201300133, June 2013

Authors

Alexander Kaiser, Samuel Zottl, Peter Bartl, Christian Leidlmair, Andreas Mauracher, Michael Probst, Stephan Denifl, Olof Echt, and Paul Scheier

Methane Adsorption on Aggregates of Fullerenes: Site-Selective Storage Capacities and Adsorption Energies

Alexander Kaiser,[a] Samuel Zöttl,[a] Peter Bartl,[a] Christian Leidlmair,[a] Andreas Mauracher,[a] Michael Probst,[a] Stephan Denifl,[a] Olof Echt,*[a, b] and Paul Scheier*[a]

Methane adsorption on positively charged aggregates of C_{60} is investigated by both mass spectrometry and computer simulations. Calculated adsorption energies of 118–281 meV are in the optimal range for high-density storage of natural gas. Groove sites, dimple sites, and the first complete adsorption shells are identified experimentally and confirmed by molecu-lar dynamics simulations, using a newly developed force field for methane–methane and fullerene–methane interaction. The effects of corrugation and curvature are discussed and compared with data for adsorption on graphite, graphene, and carbon nanotubes.

Introduction

Adsorption of hydrogen, methane, and other hydrocarbons in porous carbonaceous materials shows promise for high-density storage of hydrogen-rich molecules that may one day be used to power light-duty vehicles.[1–5] However, efficient on-board storage of hydrogen or methane presents a major technological challenge. For cars, some 10 kg of hydrogen need to be stored to achieve driving ranges greater than 300 miles (500 km). The 2017 target stated in the *2011 Interim Update of the Hydrogen Storage Engineering Center of Excellence* is to store 5.5 wt% of hydrogen at a volumetric density of 0.040 kg L^{-1}, with an ultimate target of 7.5 wt% at 0.070 kg L^{-1}.[5] The most promising alternatives for on-board storage of hydrogen are storage in form of metal hydrides, chemical compounds, or physisorption on light-weight adsorbents with large surface areas.[4] Storage of gaseous or liquid H_2 in tanks at very high pressures and/or very low temperatures is not likely to meet the targets and raises major safety issues.

For hydrogen sorption, carbon is the material of choice because of its low weight and benign environmental properties.

However, the adsorption energies on the surfaces of pristine graphene, nanotubes, and fullerenes are only 0.04–0.05 eV, well below the target of 0.1–0.4 eV (10–40 kJ mol^{-1}) set by the Hydrogen-Sorption Center of Excellence funded by the US Department of Energy.[6] Values below 0.1 eV would require cryogenic temperatures combined with high pressures, which would decrease system efficiency and increase system cost; values above 0.4 eV would require temperatures well above ambient for release of H_2 and thus compromise energy efficiency and safety.

Several strategies exist that promise increased adsorption energies; most of them involve either impurities, intrinsic defects, or multi-wall interactions, for example for adsorption sites in the interior of narrow nanotubes, or in the grooves between parallel nanotubes. Early research had indeed raised hopes that single-walled nanotubes would be able to store hydrogen at room temperature at 6 wt% and even higher.[7] However, the most promising results were found to be incorrect due to measurement errors and the presence of uncontrolled impurities, and no correlation could be established between the reported hydrogen capacities and various properties of the nanotube structures or synthesis methods.[8]

Thus, research involving nanotubes faces a fundamental dilemma: Defects are desirable because they increase adsorption energies; on the other hand, the non-uniformity of actual samples of nanotubes and the presence of unspecified defects makes it nearly impossible to determine the nature and energies of adsorption sites.[9–12] Consequently, in 2006 the Department of Energy decided to discontinue applied research and development investment in pure, undoped single-walled carbon nanotubes for vehicular hydrogen storage applications.[8] Until today, the synthesis of aligned, strictly uniform single-walled nanotubes poses a major challenge.[13] Experiments on bundles of nanotubes suffer from non-uniform tube diameters, different tube chiralities, and defects including the presence of nanosized metal and metal-oxide particles that are

[a] A. Kaiser, S. Zöttl, Dr. P. Bartl, Dr. C. Leidlmair, Dr. A. Mauracher, Prof. Dr. M. Probst, Dr. S. Denifl, Prof. Dr. O. Echt, Prof. Dr. P. Scheier
Institut für Ionenphysik und Angewandte Physik
Universität Innsbruck
Techniker Str. 25, 6020 Innsbruck (Austria)
E-mail: olof.echt@unh.edu
       paul.scheier@uibk.ac.at

[b] Prof. Dr. O. Echt
Department of Physics
University of New Hampshire
Durham, NH 03824 (USA)

used in the catalytic chemical vapor deposition (CCVD) technique, other impurities, and topological defects such as vacancies, non-hexagonal carbon rings, and the presence of uncapped tubes.

Experiments on C_{60} that can be synthesized at very high purity and free of defects offer a way out of this dilemma. Adsorption of hydrogen or methane on pristine or functionalized fullerenes has already been subject to several theoretical studies.[3,14–22] Our group computed a value of 49.5 meV for hydrogen adsorbed on pristine, isolated C_{60} by using the ωB97X-D functional without zero-point correction; the value decreased to 37.5 meV for the PBE0 functional. The values are in good agreement with a value of 32 meV obtained by using the symmetry-adapted perturbation theory,[21] and 52 meV by using local spin density approximation including the counterpoise correction.[20] The values agree closely with theoretical and experimental results obtained for H_2 adsorbed on nanotubes[23] and graphene.[24]

Higher adsorption energies have been computed for C_{60} exohedrally doped with one or more metal atoms.[3,14–18] Alkali and earth alkaline atoms are found to reside on top of hexagonal or pentagonal sites. The high electron affinity of C_{60} results in electron transfer from the metal to the fullerene, thus enhancing the binding of hydrogen to the metal atoms. The binding energies calculated for alkali or earth alkaline atoms to the fullerene exceed the cohesive energies of the bulk metals, thus avoiding undesirable clustering of metal atoms.[14–16] Adsorption energies just below 0.1 eV per hydrogen molecule have been computed for sodium,[15,18] 0.17 eV for lithium,[18] and 0.2–0.4 eV for strontium and calcium.[16]

However, experiments involving fullerenes are scarce. Saha and Deng reported that the hydrogen adsorption capacity of solid C_{60} at 77 K and 120 bar could be tripled to 13 wt % upon controlled oxidation of the sample although the adsorption isotherms indicated a heat of adsorption of only 25 meV.[25] Yamada et al. investigated hydrogen adsorption on a C_{60} monolayer deposited on a Cu(111) surface by helium scattering.[26] Thermal desorption of a hydrogen monolayer resulted in a desorption peak at 437 K from which the authors estimated a binding energy of 1.2 eV. Mauron et al. investigated adsorption of hydrogen in sodium-intercalated fullerenes (i.e., sodium fullerites).[27] They concluded that chemically bound fulleranes including $C_{60}H_{36}$ are formed in the experiment. Teprovich et al. reported on reversible chemisorption of hydrogen with lithium-doped C_{60} to form fulleranes.[28] The binding energies obtained in these latter studies[26–28] greatly exceed the optimal range for sorbent materials.[6]

An alternative experimental approach involves individual, free C_{60} molecules rather than C_{60} solids. Metallofullerene complexes such as $Ca_{32}C_{60}$ have been synthesized in helium gas and identified in mass spectra,[29] but adsorption of H_2 or other gases on these complexes has not yet been investigated.

We have recently designed a new method to study adsorption of atoms and polar or nonpolar molecules on C_{60} or C_{70} by doping cold (0.37 K), superfluid helium nanodroplets[30] with fullerene plus H_2O, NH_3, He, H_2, CH_4, or other molecules.[31–33] Nonpolar species such as He, H_2, CH_4 show a propensity to

form a commensurate layer where each carbon hexagon and pentagon adsorbs one particle although He and H_2 are sufficiently small to allow for adsorption of additional particles into the first adsorption layer.

Here, we present a first detailed study of adsorption on free aggregates of fullerenes (some results were already reported in a recent Letter[33]). We chose the C_{60}–CH_4 system because our experimental results for this system are the most comprehensive. Although hydrogen is the primary candidate for fuel cells or internal combustion engines, CH_4 is also of interest because of its low toxicity and dominance in natural gas.[1,34] Room-temperature storage on graphitic nanostructures appears more feasible for CH_4 because the physisorption energies for CH_4 are twice as large as for hydrogen; numerous experimental and theoretical investigations of CH_4 and other small hydrocarbon molecules adsorbed on graphite,[35–39] graphene,[40] nanotubes,[9,10,12,37,39,41,42] and layers of C_{60}[19] have been reported.

The experiment involves mass spectrometry, which allows us to determine the exact number of adsorption sites for fullerene aggregates containing up to five C_{60}. The nature and adsorption energies of the sites in C_{60} aggregates are determined by density functional theory (DFT) and molecular dynamics (MD) simulations. The C_{60} aggregates offer a hierarchy of adsorption sites including sites in the grooves between pairs of adjacent fullerenes that are analogous to groove sites between two parallel single-walled nanotubes and dimple sites between triplets of C_{60}, analogous to dimple sites that exist over hexagonal close-packed layers of C_{60}.[19] Calculations are presented for aggregates containing up to four C_{60} molecules. As the experimental results pertain to positively charged complexes we present calculations for neutral as well as charged systems; they display the expected[43] increase of adsorption energies upon charging. Excellent agreement between experiment and theory is obtained for the adsorption capacity in these various sites. The adsorption energy increases from 118 meV over hexagonal sites to 220 meV for groove sites and 281 meV for dimple sites; these values are in the optimal range.[6]

Results and Discussion

Experimental

A mass spectrum of helium droplets doped with C_{60} and CH_4 is displayed in Figure 1. The most prominent mass peaks are due to aggregates that contain up to five C_{60} but no CH_4 molecules. The absence of fragments such as C_{118}, C_{116} etc. that are characteristic dissociation products of highly excited fullerene dimers[44] indicates that the ionized aggregates consist of intact C_{60} units. The partial pressure of CH_4 was kept low to avoid spill-over of one series, such as C_{60}–CH_4, into the next series, $(C_{60})_2$–CH_4.

Figure 1 reveals several anomalies in the otherwise smooth ion yield of fullerene–methane complexes; labels above prominent anomalies indicate the number of methane molecules. Stars indicate mass peaks that are contaminated by contributions from doubly charged fullerene trimers, pentamers, and
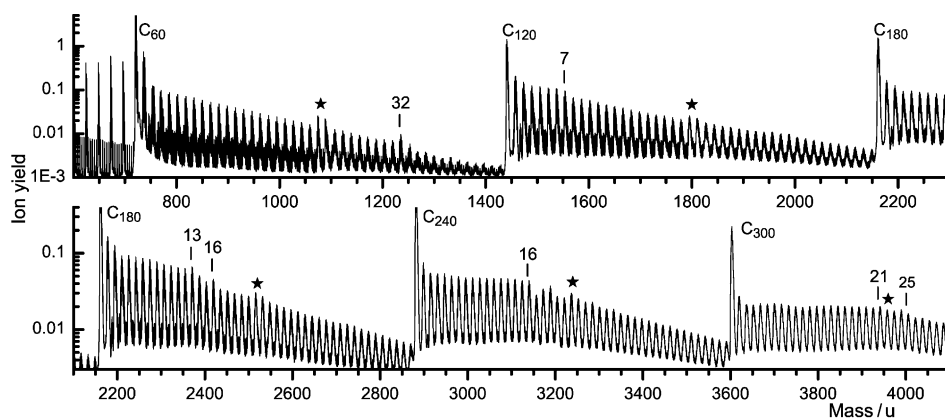
Figure 1. A mass spectrum of helium droplets doped with C_{60} and CH_4, showing the adsorption of CH_4 molecules at aggregates that contain as many as five C_{60} molecules. Some abrupt changes in the ion yield have been marked. Stars indicate contributions from doubly charged fullerene aggregates.

so on; these contaminations can be avoided by reducing the partial pressure of C_{60}.

Each mass peak in Figure 1 actually consists of several closely spaced peaks that arise from i) intramolecular dissociation of methane, ii) ion–molecule reactions in the fullerene–methane complexes, and iii) contributions from isotopologues containing one or more ^{13}C isotopes (natural abundance 1.07%). The individual peaks are well resolved for methane adsorbed on fullerene monomers and dimers. We corrected the ion yield for the (substantial) contributions from ^{13}C isotopes by using a matrix method as described in a recent publication[45] and thus obtained the abundance of isotopically pure (^{12}C only) ions.

Figure 2a displays the ion abundance of the three most intense ion series for the C_{60} monomer, namely $C_{60}(CH_4)_n^+$, $C_{60}(CH_4)_{n-1}CH_5^+$, and $C_{60}(CH_4)_{n-1}C_2H_2^+$. All three series exhibit a strong local maximum at $n=32$. Similarly, Figure 2b reveals that C_{70}–methane complexes are particularly abundant when 37 molecular units are bound to the fullerene ion.

Anomalies in the ion abundances are revealed more clearly if the distribution is divided by a smooth function. Figure 3 summarizes the corresponding data for all stoichiometric ion series, $(C_{60})_m(CH_4)^+$. The smooth functions were computed from local averages of the experimental ion abundance with Gaussian weighting.[46] By definition, these relative ion abundances average to 1; local deviations from 1 reflect anomalies in the relative dissociation energies.[47] In the special case that the heat capacities of the cluster ions are small compared to the classical equipartition value one finds that the relative ion abundances are directly proportional to the relative dissociation energies.[48] The dissociation energy D_n of a complex $C_{60}(CH_4)_n^+$ is the energy of Reaction (1):

$$C_{60}(CH_4)_n^+ \rightarrow C_{60}(CH_4)_{n-1}^+ + CH_4 - D_n \tag{1}$$

In other words, D_n is the energy required to evaporate the least-bound molecule from the complex. Thus the data in the upper panels of Figure 3 indicate that molecules in $C_{60}(CH_4)_{32}^+$ and $C_{70}(CH_4)_{37}^+$ are twice as strongly bound as the average; an

additional methane molecule adsorbed on these tightly bound complexes is a factor two more weakly bound.

The dimer ion series $(C_{60})_2(CH_4)_n^+$ (Figure 3c) shows anomalies at $n=7$ and 56. The nominal mass of $(C_{60})_2(CH_4)_{56}^+$ coincides with that of $(C_{60})_3(CH_4)_{11}^+$, but the actual masses differ by 1.41 u, so it is possible to resolve the ions. Furthermore, by adjusting the vapor pressures of C_{60} and CH_4 in the pick-up cells, the abundance of the dimer ion series could be made much larger than that of the trimer ion series.

The relative dissociation energies for CH_4 adsorbed on C_{60} trimer through hexamer ions are displayed in Figure 3d. Local maxima in the relative dissociation energies that are at least 10% above the average values occur at $n=13$ and 16 for the trimer, 16 for the tetramer, and 21 and 25 for the pentamer. An anomaly at $n=26$ for the hexamer is less significant.

Data for trimers and larger aggregates with fewer than ten adsorbed CH_4 molecules are enhanced in Figure 3d by factors 2 or 5; the dissociation energies exhibit local maxima at $n=2$
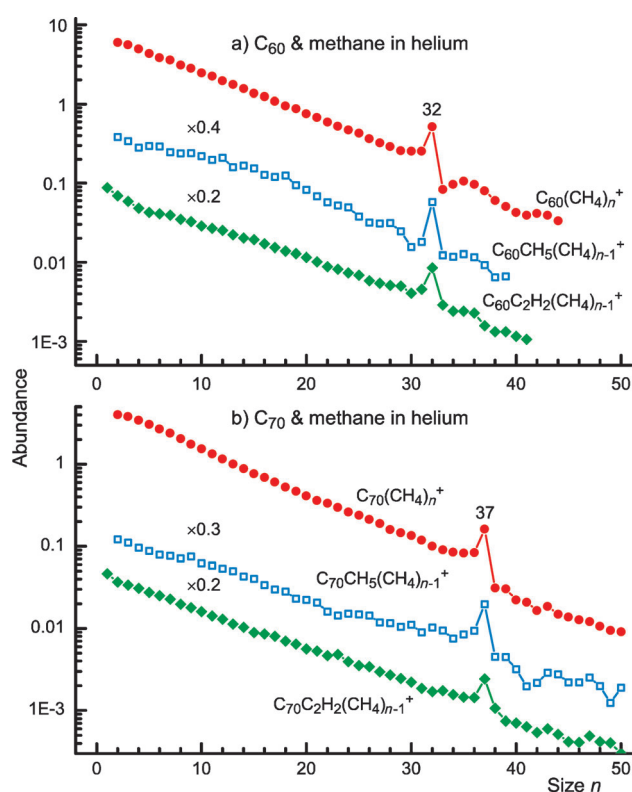

Figure 2. a) Ion abundance (corrected for contributions from species containing one or more ^{13}C atoms) of the most prominent ion series in the mass spectra, namely $C_{60}M(CH_4)_{n-1}^+$ with $M=CH_4$ (stoichiometric ions), $M=CH_5$, and $M=C_2H_2$. b) As in (a) but for C_{70}.
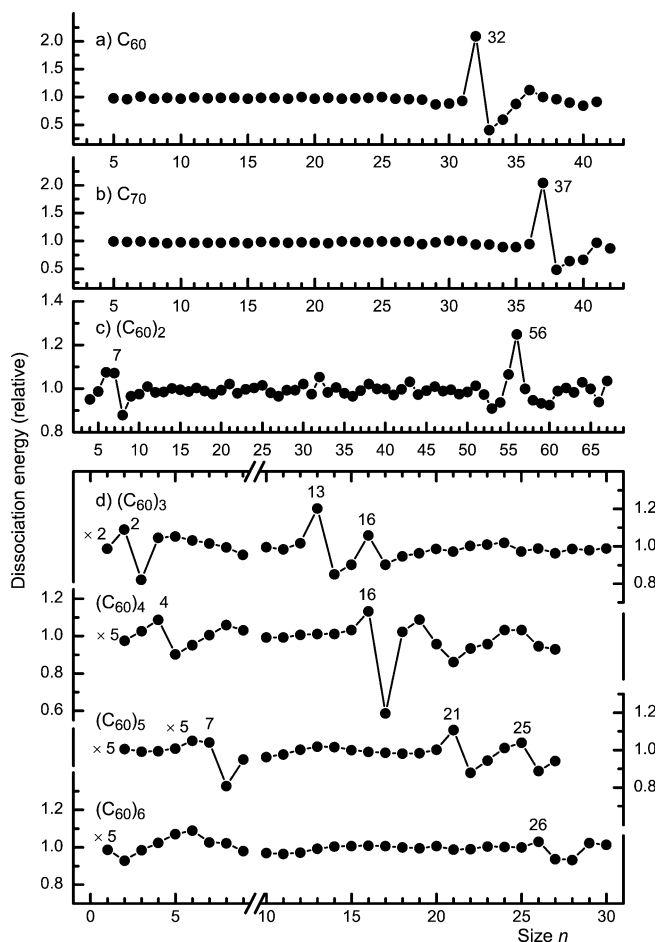
Figure 3. Ion abundance of stoichiometric ions $C_m(CH_4)_n^+$ after division by a smooth function. Anomalies in these relative abundances are expected to be approximately proportional to relative dissociation energies, that is, the energy needed to remove one CH_4 molecule from the complex.

for the C_{60} trimer, 4 for the tetramer, and 7 for the pentamer. Even though the anomalies are weak they are statistically significant because the ion abundances are quite high.[49]

All observed anomalies are listed in Table 1. In the following section we will demonstrate that these data specify the maximum numbers of molecules in specific types of adsorption sites.

Computational

We have performed molecular dynamics (MD) simulations for the adsorption of 50, 80, or 500 methane molecules on neutral or positively charged aggregates containing up to four C_{60} molecules. Most simulations were run for 400 ps with time steps of 2 fs at a temperature of 4 K. The derivation of intermolecular forces between fullerenes, between methane and neutral or charged fullerenes, and between methane molecules, is discussed at the end of this paper.

Snapshots of singly charged fullerene aggregates with 80 CH_4 molecules are shown in Figure 4; the snapshots were re-
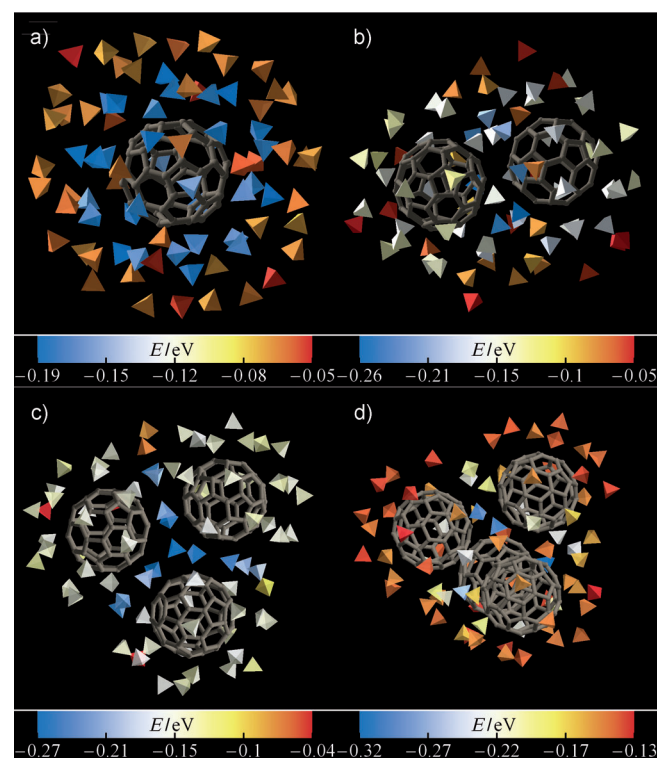

Figure 4. Energy-resolved snapshots of 80 methane molecules (shown as tetrahedra) adsorbed on charged fullerene aggregates. The monomer (a) is surrounded by a first shell of strongly bound (blue) methane molecules. The dimer (b) has the most strongly bound molecules in groove sites. For the trimer (c) and tetramer (d) dimple sites (blue) are most strongly bound, followed by other groove sites (white and yellow). The first adsorption layer is just saturated for the trimer but not yet for the tetramer.

corded at the end of simulation runs. CH_4 molecules are depicted as tetrahedra to reveal their angular orientation. The color of the tetrahedra indicates their energy E, defined as the sum over all pairwise interactions with the fullerenes and all other CH_4 molecules in the complex minus the sum of pairwise energies of the structurally unrelaxed aggregate with one missing CH_4 molecule. According to this definition, the most strongly bound molecules in a complex have the lowest (most negative) values of E. We refer to $-E$ as the binding energy.[50] From Figure 4 one sees that the binding energies for the strongest-bound molecules increase as the number of C_{60} mol-

Table 1. Anomalies observed in the ion abundance together with features extracted from the computed energy and spatial distributions of methane molecules adsorbed on charged C_{60} aggregates.

C_{60} aggregate	Number of sites			
	experiment	theory		
		dimple	groove	full layer
monomer	32	–	–	32
dimer	7, 56	–	7	58
trimer	2, 13, 16	(2)	13	≈80
tetramer	4, 16	4	17	≈100
pentamer	7, 21, 25	–	–	–

ecules in the complex increases (note that each panel in Figure 4 has a different energy-to-color conversion scale).

The first solvation shell of C_{60}^+ is easily visible in Figure 4a; the 32 most strongly bound molecules (colored blue) are adsorbed over the 12 pentagonal and 20 hexagonal faces. For the dimer (Figure 4b), the most strongly bound (blue) CH_4 molecules reside in the waist region; these adsorption sites will be referred to as groove sites. Other molecules in the first adsorption layer of the dimer are less strongly bound; they are colored white.

The snapshot of the trimer (Figure 4c) reveals the enhanced binding in groove sites. Two of these groove sites offer particularly strong binding, namely the sites near the three-fold symmetry axis, so-called dimple sites (above and below the plane defined by the fullerenes). The C_{60} tetramer (Figure 4d) has four such dimple sites.

Snapshots are not necessarily representative of the system over long times. To extract more reliable, quantitative data we have analyzed the geometry and energy of the systems over the last 50 ps of each simulation, with snapshots stored at increments of 1 ps. The histogram in Figure 5 displays the distri-
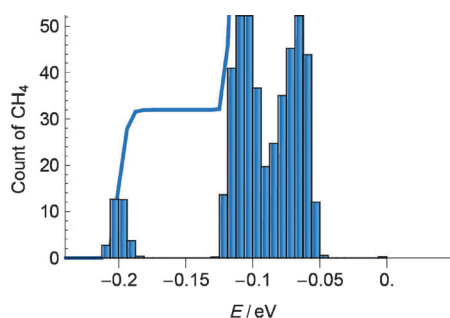

Figure 5. Histogram of the number of CH_4 molecules with binding energies E for $C_{60}(CH_4)_{500}^+$. The solid line represents the cumulative sum of all molecules with energies smaller than E.

bution of energies E for $C_{60}(CH_4)_{500}^+$. The 32 molecules that reside over the 20 hexagonal and 12 pentagonal faces form the narrow peak at $E = -0.2$ eV. The adsorption energies of the two sites differ by several percent; the sites will be characterized in more detail further below. The solid line in Figure 5 represents the cumulative sum of molecules with energies smaller than the indicated bin-energy E. The large energy gap in the histogram corresponds to the broad plateau in the cumulative sum. In the following we will merely show these cumulative sums, which allows for less congested Figures.

Figure 6 displays the energy distributions for the C_{60} monomer through tetramer for the most strongly bound CH_4 molecules, where the energy of a CH_4 molecule is defined as the sum over all pair-interactions with C_{60} and other CH_4 molecules. The dimer features a distinct plateau at $n = 7$, the trimer at $n = 13$, and the tetramer at $n = 4$ and 17. The distinctness of the plateaus depends slightly on the number of CH_4 molecules in the simulation (either 50, 80, or 500). For C_{60} aggregates (excluding the monomer) with 500 CH_4 molecules the plateaus become somewhat blurred because the contributions from the
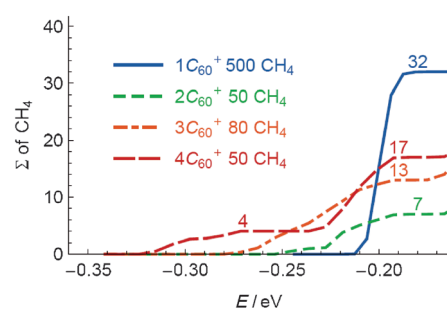

Figure 6. Counting the number of molecules in the adsorption layer of the charged C_{60} monomer through tetramer: The cumulative sums of molecules derived from the energy distributions (cf. Figure 5) reach plateaus when specific types of adsorption sites become saturated. One sees that there are four dimple sites for the tetramer; 7, 13, and 17 groove sites (including dimple sites) for the dimer through tetramer; and 32 face-centered sites for the monomer.

large number of molecules in outer layers are subject to thermal fluctuations. However, these simulations are valuable because they reveal additional plateaus at about 55–60 for the dimer, about 80 for the trimer, and about 100 for the tetramer.[51]

The energies of the four curves in Figure 6 cannot be compared directly to each other because of different occupations of the second and third solvation shells in our calculations. More insight was obtained by computing the energetics and geometry of a single CH_4 molecule adsorbed on charged C_{60} aggregates; results are listed in Table 2. For C_{60}^+, hexagonal sites (117.8 meV) are preferred to pentagonal sites (107.9 meV)

Table 2. Computational results for a single methane molecule adsorbed on a charged fullerene aggregate. $\min\{d\}$ is the distance to the center of the nearest fullerene. Values were obtained by using the classical force field (as used in the MD simulation) and an optimization procedure.

C_{60} aggregate	Site	Energy [meV]	$\min\{d\}$ [Å]
monomer	pentagon	107.9	6.70
monomer	hexagon	117.8	6.57
dimer	groove	218.4	6.57
trimer	dimple	280.9	6.71

as already observed for H_2 on C_{60}.[45] In its optimal configuration, CH_4 resides 6.57 Å away from the center of the fullerene in the so-called "face" geometry. This structure was discussed for carbon nanotubes by Akai and Saito.[42] They reported a maximum adsorption energy of 90 meV on the outside of the tube over a nanotube-hexagon and 96 meV on graphene. A comparative study of various dispersion corrected functionals applied to the methane–graphene system yielded adsorption energies in the range of 140–300 meV in the "face" geometry, denoted as "1d" by Thierfelder et al.[40] Yang et al.[36] studied CH_4 adsorption on graphite with ab initio methods and reported 118 meV in the "face" configuration at low coverage, whereas Albesa et al.[38] reported a heat of adsorption of 12.6 kJ mol^{-1} (131 meV) using Monte Carlo simulations. An ex-

perimental value of $11.3 \, kJ\,mol^{-1}$ (117 meV) was reported by Bienfait et al.[10] for the isosteric heat of adsorption of CH_4 on the external surface of a single-walled nanotube bundle. Our value of 117.8 meV agrees well with those data. As expected, adsorption energies decrease from flat to curved surfaces.

The adsorption energy in a groove site of a fullerene dimer (218.4 meV) is 85 % larger than the energy in a single hexagonal site. The energy does not double because the perfect "face" arrangement of the hydrogen atoms over hexagons is not possible for groove sites. MP2 calculations of methane on carbon nanotubes predicted 126 meV for a single tube and 243 meV for a nanotube groove,[37] an increase of 93 %. Absolute values are slightly larger compared to C_{60} due to the lower curvature. The adsorption energy increases to 280.9 meV for the $(C_{60})_3^+$ dimple site, 2.4 times the value over a hexagon of the C_{60} monomer ion. A geometry where one of the four vertices of methane points towards the center of all three fullerenes has been found; the minimal distance of the methane carbon atom to the center of one of the fullerenes increases from 6.57 for the monomer to 6.71 Å for the trimer.

The bare C_{60} dimer ion deserves some discussion. Its optimized (B3LYP/6-31g(d,p) without CP[52] correction) structure is displayed in Figure 7. For a better view both spheres were cropped; only the two abutting hemispheres are shown. Both molecules are tilted, but the hexagonal faces stay nearly paral-
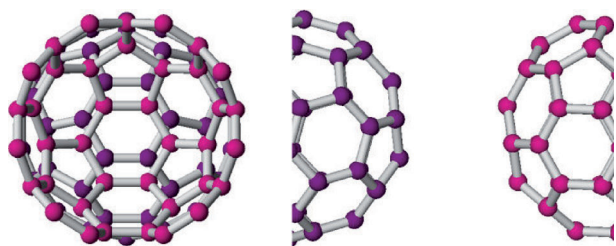

Figure 7. Part of the optimized fullerene dimer ion in front (axial) view (left) and side view (right). The fullerenes were cropped for the sake of clearer visualization.

lel; no lateral rotation was observed. A very similar structure was called the H–HH configuration and reported to have the highest binding energy for the neutral dimer.[53] In this configuration a hexagon (H) is opposite a bond between two hexagons (HH). The calculated binding energy is −449 meV, stronger than −338 meV calculated by Zettergren et al.,[54] but the equilibrium distance (10.24 Å) is the same. For comparison, an optimization by using the dispersion-corrected functional ωB97X-D yields a larger binding energy of −639 meV at a similar geometry and a smaller distance of 9.59 Å.

What types of adsorption sites give rise to the plateaus in the energy distributions (Figure 6), that is, the gaps in the corresponding energy histograms? So far we inferred the nature of adsorption sites from individual snapshots. Statistically more accurate information is derived from spatial distributions that count molecules in specific adsorption sites. Let $\{d\}$ denote the set of distances of a specific methane molecule from the centers of all fullerenes in the aggregate, and min$\{d\}$ the distance

from the nearest C_{60}. For the monomer, min$\{d\}$ is simply the distance from the center of the fullerene; for the dimer min$\{d\}$ is the smaller of the two distances, etc. Gaps in a histogram plotted versus min$\{d\}$ will thus reveal geometrically distinct adsorption layers. The corresponding cumulative sums of these distributions, computed for 500 CH_4 molecules adsorbed on C_{60} and its aggregates, are shown in Figure 8. All aggregates feature distinct plateaus between min$\{d\} = 7.0$ Å, where the
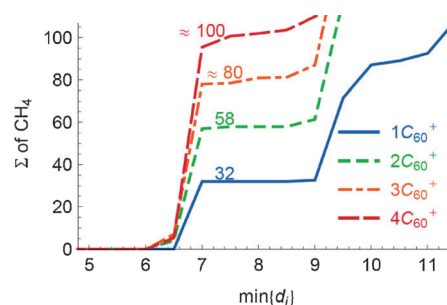

Figure 8. Cumulative sums of molecules derived from the spatial distributions reach plateaus when the first or, for the monomer, second adsorption layer are completed. min$\{d\}$ denotes the distance of a given CH_4 molecule from the center of the nearest fullerene.

first adsorption layer is completed, and 9.0 Å, where the second adsorption layer starts to build. The equilibrium distance of a single methane molecule adsorbed on C_{60}^+ ranges from 6.5 to 6.7 Å depending on the site and orientation of the molecule; the mean distance of the 32 nearest methane molecules in a simulation of $C_{60}(CH_4)_{50}^+$ is 6.69 Å.

For the C_{60} dimer Figure 8 features a plateau at $n = 58$ for the first adsorption layer, which agrees with the above-mentioned, less distinct plateau at about 55 to 60 in the energy distribution and the experimentally observed, distinct anomaly in the ion abundance at $n = 56$. Unfortunately, it is not possible to experimentally test the predictions for the completion of the first adsorption layers at $n \approx 80$ and ≈ 100 for the C_{60} trimer and tetramer because of strong mass spectral interference with ions that contain additional C_{60} but fewer methane molecules.

The spatial distributions in Figure 8 do not reveal the number of groove or dimple sites because min$\{d\}$ has very nearly the same value for all molecules in the first adsorption layer. Instead, the following procedure is applied: As before, let $\{d_1, d_2, d_3, \ldots\}$ denote the distances of a specific CH_4 molecule to the centers of the fullerenes in the aggregate. Let d_i and d_j denote the two smallest values in this set. The molecule in question resides in a groove site if $|d_i - d_j| < \varepsilon$, where ε is a small, somewhat arbitrarily chosen distance that describes the approximate width of the groove region. For the dimer, the algorithm defines the region that encloses the plane bisecting the dimer axis. For the trimer and tetramer the regions defined as groove regions are illustrated in Figure 9, choosing $\varepsilon = 1$ Å. Note that our definition does not limit the groove regions to the first adsorption layer, but the value of min$\{d\}$
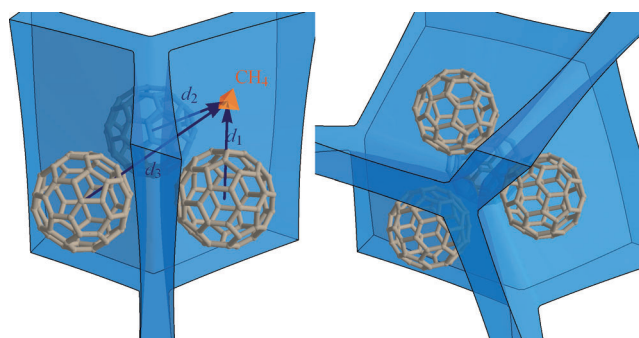
Figure 9. Groove sites for the a) trimer and b) tetramer ion, defined as the regions for which the distances to the two nearest C_{60} molecule are identical within 1 Å.

Figure 10. Location of CH_4 molecules in groove sites of a fullerene dimer for different temperatures, showing a high degree of order at low temperatures. For each 1 ps time step of the simulation, the position of all molecules in the groove region is projected onto the plane that bisects the dimer axis.

helps to distinguish between groove sites that are part of the first adsorption layer and those that are further away.

The calculated number of groove sites in the first adsorption layer is 7, 13, and 17 for the dimer through tetramer. The first two values are in perfect agreement with the experimental data (see Table 1); the value for the tetramer exceeds the experimental value by just one. The computed values are robust with respect to the choice of ε although ε has to be large enough to filter out small structural fluctuations.

The criterion for the definition of groove sites is easily extended to count the number of CH_4 molecules in dimple sites (i.e., sites that have three nearest C_{60} molecules at approximately equal distances; they form a subset of groove sites). The results are, not surprisingly, $n = 2$ for the trimer and 4 for the tetramer. The dimple sites of the tetramer are significantly more strongly bound than the remaining 13 groove sites; they form a plateau in the energy distribution, see Figure 6. On the other hand, the two dimple sites of the trimer do not form a distinct plateau in the energy distribution. This is probably due to contributions from the remaining molecules in $(C_{60})_3(CH_4)_{80}^+$ that are subject to thermal energy fluctuations.

Simulations discussed so far were performed at 4 K. The effect of temperature has been studied for the C_{60} dimer with 500 adsorbed CH_4 molecules. Figure 10 shows the positions of all CH_4 molecules that reside in the groove region, projected onto the plane that bisects the dimer axis. Projections were recorded every picosecond for the whole duration of a simulation. The pattern at 20 K is very regular. The CH_4 molecules are arranged in a circular pattern and strongly localized, that is, there is radial and angular order, even far away from the innermost ring of seven molecules. At 30 K one still sees radial order in the first two or three rings, but at 40 K most of the order is lost except for the innermost ring.

At 10 K the position of the seven innermost methane molecules has changed. One of them (near the top in Figure 10) is displaced outwards; the remaining six form a nearly regular hexagon. This could perhaps signal that the packing of seven molecules in the groove is slightly too tight. To further investigate this, geometries were optimized with six, seven, and eight methane molecules in the groove. Starting at different temperatures we performed a step by step annealing in the
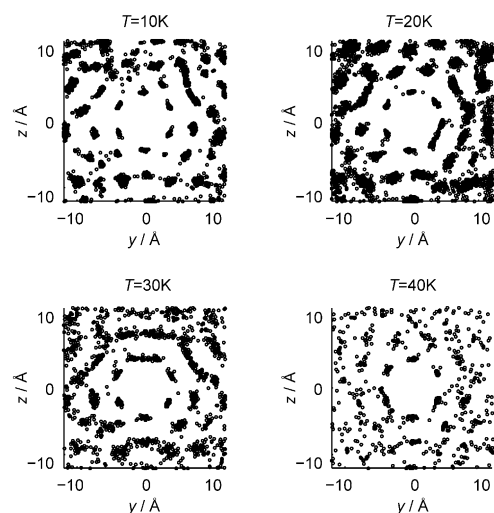
MD runs and a final optimization run at 0 K. Starting at 30 K with six methane molecules, a highly symmetric structure is revealed that also reflects the symmetry of the substrate as shown in Figure 11 a. The orientation of the molecules alternates; either one (resembling a "goblet") or two (resembling a "jumper" with hands up) hydrogen atoms are oriented inward. For a single molecule in the groove the jumper orientation is more favorable than the goblet configuration. The same was found for methane in grooves of nanotubes[12].
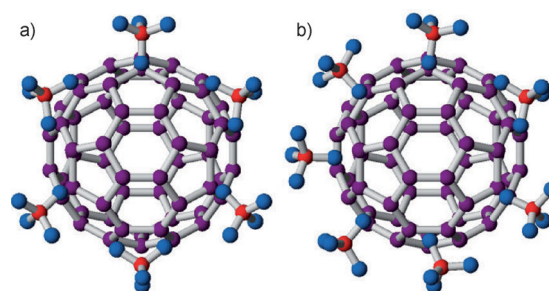

Figure 11. Methane molecules in groove sites of the C_{60} dimer ion with a) six or b) seven CH_4 molecules. In this axial view the front fullerene is not shown to reveal the orientation of the adsorbate molecules more clearly.

For seven CH_4 molecules the result depends on the initial temperature of the simulation. Starting at or below 20 K one obtains the result shown in Figure 11 b; all seven molecules reside in the groove with six in the goblet and one in the jumper orientation. If the simulation starts at 30 K, one of the seven molecules is pushed out of the groove to a nearby hexagon upon cooling, yielding a lower energy. The final arrangement resembles that in Figure 10 at 10 K. Simulations with eight CH_4 molecules invariably result in one molecule being far outside the groove region. The average adsorption energies

per molecule are 208, 194, and 184 meV for six, seven, and eight CH_4 molecules, respectively.

Information about the structural order of the CH_4 molecules in the grooves of the trimer may be inferred from their number, 13. The trimer has two dimple sites and three separate grooves. If the two dimple sites were occupied 11 molecules would have to reside in the three grooves, which does not allow for any regular arrangement. Instead, the molecules in the dimple sites might be displaced from the three-fold symmetry axis of the trimer, which will negatively impact on their binding energies. This may explain the absence of an energy gap in the calculated energy distribution, see Figure 6. Indeed, from a visual inspection of the MD trajectories we find that one of the dimple-site molecules is displaced from the exact dimple-site position.

For the tetramer, the calculated number of 17 molecules in groove sites including four in dimple sites would imply that 13 molecules reside in six grooves, again defying any regular arrangement. However, the experimental number is 16, which does allow for a highly symmetric arrangement, with four molecules in dimple sites plus two in each groove. The anomaly in the ion abundance and relative dissociation energy for this arrangement is accordingly large, see Figures 1 and 3d.

Conclusions

Intriguing new structures were identified by synthesizing fullerene–methane complexes within superfluid helium nanodroplets. These structures consist of methane molecules weakly adsorbed on charged fullerenes at moderate distances. Due to the high curvature of the fullerene a commensurate phase is possible, where each hexagon and pentagon of C_{60}^+ adsorbs exactly one molecule. For the C_{60} dimer, trimer, and tetramer ion the number of groove and dimple sites could be measured; the results agree closely with MD simulations. For the MD simulations a force field for fullerene–methane and methane–methane interactions was developed. Binding energies for adsorption on hexagons, pentagons, and in groove or dimple sites have been calculated and are in good agreement with corresponding data on nanotubes and other carbonaceous structures. A fullerene dimer supports six or seven molecules in the groove region at approximately 80% higher binding energies than in the first adsorption shell of C_{60}^+; the trimer ion offers dimple sites that are 2.4 times as strongly bound.

Experimental Section

Neutral helium nanodroplets were produced by expanding helium (purity 99.9999%) from a stagnation pressure of 2 MPa through a 5 μm nozzle, cooled to about 8 K, into vacuum. The estimated average number of helium atoms per droplet formed in the expansion was of the order of 5×10^5; the droplets were superfluid with a temperature of approximately 0.37 K.[30] The resulting supersonic beam was skimmed by using a 0.8 mm conical skimmer, located 8 mm downstream from the nozzle. The skimmed beam traversed a 20 cm long differentially pumped pickup region containing methane (Linde 99.995%) at partial pressures ranging from 1×10^{-3}

to 4×10^{-3} Pa. A small amount of C_{60} (MER Corp., purity 99.9%) or C_{70} (SES Research, 99%) was vaporized into the pickup region from a crucible.

After the pickup region the doped helium droplets passed a region in which they were ionized by electron impact at 70 eV. Cations were accelerated to 40 eV into the extraction region of a commercial time-of-flight mass spectrometer equipped with a reflectron (Tofwerk AG, model HTOF); its mass resolution was about $\Delta m/m = 1{:}5000$. The base pressure in the mass spectrometer was 10^{-5} Pa. The ions were extracted at 90° into the field-free region of the spectrometer by using a pulsed extraction voltage. At the end of the field-free region they entered a two-stage reflectron, which reflected them towards a microchannel plate detector operated in single-ion-counting mode. Further experimental details have been described elsewhere.[32,55]

Computational methods

MD simulations were performed at a temperature of 4.0 K within the NVT ensemble using a Nosé–Hoover[56] thermostat. Quantum chemically [B3LYP/6-31g(d,p)] optimized geometries of fullerene mono-, di-, tri-, and tetramers were space-fixed in the simulation. The fullerenes were surrounded by 50, 80, or 500 randomly distributed methane molecules. The initial condition is best described as a sparse cloud of methane molecules surrounding the fullerenes.

We used periodic boundary conditions with a large box size (1000 Å) to simulate vacuum conditions. In all simulations one of the fullerenes carried a charge of +1, distributed evenly on the C atoms. The methane molecules were treated as rigid bodies. The system was given enough time (400 ps) to obtain a stable configuration. We operated with an integration time step of 2 fs and stored snapshots of the trajectory every picosecond. A cutoff of 30 Å ensured a correct treatment of the long-range effects.

A new force-field for the C_{60}–CH_4, C_{60}^+–CH_4, as well as for the CH_4–CH_4 interactions was developed. The $C_{60}^{0,+}$–CH_4 energy surfaces of the neutral and charge species were sampled with DFT calculations by using the dispersion-corrected ωB97X-D functional.[57] This functional has been shown to be a suitable tool to describe weak interactions such as hydrogen bonds and induced polarization with an accuracy comparable to MP2 and has proven its efficiency for various molecular systems.[58] To sample the $C_{60}^{0,+}$–CH_4 potential surface, five sites have been chosen: The centers of a hexagonal face, a pentagonal face, the bond between two hexagons, the bond between a hexagon and a pentagon, and the position of a C atom. One CH_4 molecule was placed over these sites in three different rotational orientations and its distance d from the fullerene center was varied from $d = 6.5$ to 15.5 Å; in total, 915 pair energies were calculated. The interaction was assumed to be zero at $d = 30$ Å, and the total energies where shifted by the respective dissociation energies. It turned out that the potential energy depended considerably on the orientation of the CH_4 molecule (by about 50 meV), thus prohibiting to approximate CH_4 single sites ("united atom") in the energy expression. In a fully relaxed optimization of the neutral C_{60}–CH_4 system the deformation energy of CH_4 was only 1.8 meV, the total energy differed by only 0.2 eV, and the distance of the CH_4 C atom to the center of C_{60} changed by −0.03 Å only while simultaneously tilting slightly to one side. The adsorption energy agreed within 2% with the value of the non-relaxed system.

The CH_4–CH_4 potential surface was sampled in a similar procedure using coupled cluster calculations with single and double substitu-

tions (CCSD[59]) in combination with the cc-pVTZ basis set.[60] The basis set superposition error was accounted for by the counterpoise method. A total number of 816 points of the potential energy surface were calculated by scanning distances between 3 and 13 Å in 16 configurations. The CH_4–CH_4 interaction also depended strongly on the orientation of the molecules to each other. The CH_4–CH_4 system is ideally suited for benchmarking the ωB97X-D functional by comparison to our CCSD results. We found that ωB97X-D yielded relatively good adsorption distances within 5% of the CCSD results. The trends in the adsorption energies were conserved with the ωB97X-D functional, but the absolute values were overestimated by a factor of two.

$C_{60}^{0,+}$–CH_4 and CH_4–CH_4 force fields were then obtained by fitting the parameters of atom–atom pair potentials to the potential energy values. The functions and corresponding parameters are collected in Table 3. A thorough evaluation of the force field and the fitting will be given elsewhere.

Table 3. Pair potential energy functions, $V(r)$, and values of the empirical coefficients C_{12} (in eV Å^{12}), C_{10} (in eV Å^{10}), C_6 (in eV Å^6), A (in eV), and ρ (in Å).

System	Interaction	Pair potential	Values of the parameters			
C_{60}^+–CH_4	C–C	C_{12}/r^{12}-C_6/r^6	C_{12}	60316.2	C_6	56.0586
C_{60}^+–CH_4	C–H	C_{12}/r^{12}-C_6/r^6	C_{12}	1508.7	C_6	0.86022
C_{60}–CH_4	C–C	C_{10}/r^{10}-C_6/r^6	C_{10}	4178.45	C_6	52.1998
C_{60}–CH_4	C–H	C_{10}/r^{10}-C_6/r^6	C_{10}	301.922	C_6	2.104
CH_4–CH_4	C–C	C_{10}/r^{10}-C_6/r^6	C_{10}	3.021	C_6	22.2
CH_4–CH_4	C–H	$A e^{-r/\rho}$-C_6/r^6	A 21.34	ρ 0.4071	C_6 8.411	
CH_4–CH_4	H–H	$A e^{-r/\rho}$-C_6/r^6	A 6.708	ρ 0.3603	C_6 0.3642	

The C_{60}–C_{60} interactions were not treated with a force field during the MD-simulations. The fullerenes were kept fixed at optimized geometries [B3LYP/6-31G(d,p)] for the mono-, di-, trimer, and for the tetramer an additional fullerene was inserted manually to match tetrahedral symmetry at the average C_{60}–C_{60} distance of the trimer. We did not expect significant improvements upon using relaxed fullerenes because of the large binding energy of the C_{60} dimer compared to C_{60}–CH_4.

All calculations were performed with the 6-31g(d,p) basis set,[52,61] which includes polarization functions.[62] The Gaussian 09 A.02 program package[63] was used for the quantum chemical calculations and the MD simulations were performed with the DL_POLY[64] software.

Acknowledgements

[1] L. Schlapbach, A. Züttel, *Nature* **2001**, *414*, 353–358.
[2] G. W. Crabtree, M. S. Dresselhaus, *MRS Bull.* **2008**, *33*, 421–428; C. J. Liu, U. Burghaus, F. Besenbacher, Z. L. Wang, *ACS Nano* **2010**, *4*, 5517–5526.
[3] P. Jena, *J. Phys. Chem. Lett.* **2011**, *2*, 206–211.
[4] US Department of Energy, *Energy Efficiency & Renewable Energy/Hydrogen Storage*, http://www1.eere.energy.gov/hydrogenandfuelcells/storage/current_technology.html, accessed January 2013.
[5] Hydrogen Storage Engineering Center of Excellence, *Hydrogen Storage Engineering Center of Excellence (HSECoE)* http://hsecoe.srs.gov/technicalgap.html, accessed January 2013.
[6] National Renewable Energy Laboratory, Golden, Colorado, *HSCoE Final Report Executive Summary*, http://www1.eere.energy.gov/hydrogenandfuelcells/pdfs/hydrogen_sorption_coe_final_report.pdf, September 30 **2010**.
[7] A. C. Dillon, K. M. Jones, T. A. Bekkedahl, C. H. Kiang, D. S. Bethune, M. J. Heben, *Nature* **1997**, *386*, 377; Y. Ye, C. C. Ahn, C. Witham, B. Fultz, J. Liu, A. G. Rinzler, D. Colbert, K. A. Smith, R. E. Smalley, *Appl. Phys. Lett.* **1999**, *74*, 2307–2309.
[8] US Department of Energy, *Go/No-Go Decision: Pure, Undoped Single-Walled Carbon Nanotubes for Vehicular Hydrogen Storage*, www.hydrogen.energy.gov/pdfs/go_no_go_nanotubes.pdf, October 2006.
[9] W. Shi, J. K. Johnson, *Phys. Rev. Lett.* **2003**, *91*, 015504; M. R. LaBrosse, W. Shi, J. K. Johnson, *Langmuir* **2008**, *24*, 9430–9439; M. R. LaBrosse, J. K. Johnson, *J. Phys. Chem. C* **2010**, *114*, 7602–7610.
[10] M. Bienfait, P. Zeppenfeld, N. Dupont-Pavlovsky, M. Muris, M. R. Johnson, T. Wilson, M. DePies, O. E. Vilches, *Phys. Rev. B* **2004**, *70*, 035410.
[11] A. Nikitin, X. L. Li, Z. Y. Zhang, H. Ogasawara, H. J. Dai, A. Nilsson, *Nano Lett.* **2008**, *8*, 162–167; M. Arai, S. Utsumi, M. Kanamaru, K. Urita, T. Fujimori, N. Yoshizawa, D. Noguchi, K. Nishiyama, Y. Hattori, F. Okino, T. Ohba, H. Tanaka, H. Kanoh, K. Kaneko, *Nano Lett.* **2009**, *9*, 3694–3698.
[12] A. G. Albesa, E. A. Fertitta, J. L. Vicente, *Langmuir* **2010**, *26*, 786–795.
[13] Q. Zhang, J.-Q. Huang, M.-Q. Zhao, W.-Z. Qian, F. Wei, *ChemSusChem* **2011**, *4*, 864–889; G. Centi, S. Perathoner, *ChemSusChem* **2011**, *4*, 913–925; J.-P. Tessonnier, D. S. Su, *ChemSusChem* **2011**, *4*, 824–847.
[14] Q. Sun, P. Jena, Q. Wang, M. Marquez, *J. Am. Chem. Soc.* **2006**, *128*, 9741–9745.
[15] K. R. S. Chandrakumar, S. K. Ghosh, *Nano Lett.* **2008**, *8*, 13–19.
[16] M. Yoon, S. Y. Yang, C. Hicke, E. Wang, D. Geohegan, Z. Y. Zhang, *Phys. Rev. Lett.* **2008**, *100*, 206806.
[17] Q. Wang, Q. Sun, P. Jena, Y. Kawazoe, *J. Chem. Theory Comput.* **2009**, *5*, 374–379; Q. Wang, P. Jena, *J. Phys. Chem. Lett.* **2012**, *3*, 1084–1088.
[18] W. Liu, Y. H. Zhao, Y. Li, Q. Jiang, E. J. Lavernia, *J. Phys. Chem. C* **2009**, *113*, 2028–2033.
[19] S. M. Gatica, M. K. Kostov, M. W. Cole, *Phys. Rev. B* **2008**, *78*, 205417; R. A. Trasca, M. W. Cole, T. Coffey, J. Krim, *Phys. Rev. E* **2008**, *77*, 041603.
[20] P. A. Denis, *J. Phys. Chem. C* **2008**, *112*, 2791–2796.
[21] T. Korona, A. Hesselmann, H. Dodziuk, *J. Chem. Theory Comput.* **2009**, *5*, 1585–1596.
[22] M. Yoon, S. Y. Yang, Z. Y. Zhang, *J. Chem. Phys.* **2009**, *131*, 064707; T. T. Vehviläinen, M. G. Ganchenkova, L. E. Oikkonen, R. M. Nieminen, *Phys. Rev. B* **2011**, *84*, 085447.
[23] K. A. Williams, B. K. Pradhan, P. C. Eklund, M. K. Kostov, M. W. Cole, *Phys. Rev. Lett.* **2002**, *88*, 165502; C. M. Brown, T. Yildirim, D. A. Neumann, M. J. Heben, T. Gennett, A. C. Dillon, J. L. Alleman, J. E. Fischer, *Chem. Phys. Lett.* **2000**, *329*, 311–316; J. S. Arellano, L. M. Molina, A. Rubio, M. J. Lopez, J. A. Alonso, *J. Chem. Phys.* **2002**, *117*, 2281–2288.
[24] Y. Okamoto, *J. Phys. Chem. A* **2001**, *105*, 7634–7637; A. Ferre-Vilaplana, *J. Chem. Phys.* **2005**, *122*, 104709; M. Rubeš, O. Bludský, *ChemPhysChem* **2009**, *10*, 1868–1873.
[25] D. Saha, S. G. Deng, *Carbon* **2010**, *48*, 3471–3476.
[26] Y. Yamada, Y. Satake, K. Watanabe, Y. Yokoyama, R. Okada, M. Sasaki, *Phys. Rev. B* **2011**, *84*, 235425.
[27] P. Mauron, A. Remhof, A. Bliersbach, A. Borgschulte, A. Züttel, D. Sheptyakov, M. Gaboardi, D. Choucair, M. Pontiroli, M. Aramini, A. Gorreri, M. Ricco, *Int. J. Hydrogen Energy* **2012**, *37*, 14307–14314.

[28] J. A. Teprovich, M. S. Wellons, R. Lascola, S. J. Hwang, P. A. Ward, R. N. Compton, R. Zidan, *Nano Lett.* **2012**, *12*, 582 – 589.

[29] U. Zimmermann, N. Malinowski, A. Burkhardt, T. P. Martin, *Carbon* **1995**, *33*, 995 – 1006; A. Enders, N. Malinowski, D. Ievlev, E. Zurek, J. Autschbach, K. Kern, *J. Chem. Phys.* **2006**, *125*, 191102.

[30] J. P. Toennies, A. F. Vilesov, *Angew. Chem.* **2004**, *116*, 2674 – 2702; *Angew. Chem. Int. Ed.* **2004**, *43*, 2622 – 2648.

[31] S. Denifl, F. Zappa, I. Mähr, F. Ferreira da Silva, A. Aleem, A. Mauracher, M. Probst, J. Urban, P. Mach, A. Bacher, O. Echt, T. D. Märk, P. Scheier, *Angew. Chem.* **2009**, *121*, 9102 – 9105; *Angew. Chem. Int. Ed.* **2009**, *48*, 8940 – 8943; S. Denifl, F. Zappa, I. Mähr, A. Mauracher, M. Probst, J. Urban, P. Mach, A. Bacher, D. K. Bohme, O. Echt, T. D. Märk, P. Scheier, *J. Chem. Phys.* **2010**, *132*, 234307; H. Schöbel, C. Leidlmair, P. Bartl, A. Aleem, M. Hager, O. Echt, T. D. Märk, P. Scheier, *Phys. Chem. Chem. Phys.* **2011**, *13*, 1092 – 1098; C. Leidlmair, Y. Wang, P. Bartl, H. Schöbel, S. Denifl, M. Probst, M. Alcamí, F. Martín, H. Zettergren, K. Hansen, O. Echt, P. Scheier, *Phys. Rev. Lett.* **2012**, *108*, 076101.

[32] C. Leidlmair, P. Bartl, H. Schöbel, S. Denifl, M. Probst, P. Scheier, O. Echt, *Astrophys. J. Lett.* **2011**, *738*, L4.

[33] S. Zöttl, A. Kaiser, P. Bartl, C. Leidlmair, A. Mauracher, M. Probst, S. Denifl, O. Echt, P. Scheier, *J. Phys. Chem. Lett.* **2012**, *3*, 2598 – 2603.

[34] T. Düren, L. Sarkisov, O. M. Yaghi, R. Q. Snurr, *Langmuir* **2004**, *20*, 2683 – 2689; A. V. Vakhrushev, M. V. Suyetin, *Nanotechnology* **2009**, *20*, 125602; Y. M. Li, G. A. Somorjai, *Nano Lett.* **2010**, *10*, 2289 – 2295.

[35] J. Piper, J. A. Morrison, *Phys. Rev. B* **1984**, *30*, 3486 – 3489.

[36] S. H. Yang, L. Z. Ouyang, J. M. Phillips, W. Y. Ching, *Phys. Rev. B* **2006**, *73*, 165407.

[37] A. Ricca, C. W. Bauschlicher, *Chem. Phys.* **2006**, *324*, 455 – 458.

[38] A. G. Albesa, J. L. Llanos, J. L. Vicente, *Langmuir* **2008**, *24*, 3836 – 3840.

[39] O. O. Adisa, B. J. Cox, J. M. Hill, *Carbon* **2011**, *49*, 3212 – 3218.

[40] C. Thierfelder, M. Witte, S. Blankenburg, E. Rauls, W. G. Schmidt, *Surf. Sci.* **2011**, *605*, 746 – 749.

[41] M. Muris, N. Dupont-Pavlovsky, M. Bienfait, P. Zeppenfeld, *Surf. Sci.* **2001**, *492*, 67 – 74; M.K. Kostov, M.M. Calbi, M.W. Cole, *Phys. Rev. B* **2003**, *68*, 245403; A. D. Lueking, M. W. Cole, *Phys. Rev. B* **2007**, *75*, 195425; J. Wu, F. Hagelberg, *Phys. Rev. B* **2010**, *81*, 155407.

[42] Y. Akai, S. Saito, *Jpn. J. Appl. Phys. Part 1* **2003**, *42*, 640 – 644.

[43] M. Yoon, S. Y. Yang, E. Wang, Z. Y. Zhang, *Nano Lett.* **2007**, *7*, 2578 – 2583.

[44] F. Rohmund, E. E. B. Campbell, O. Knospe, G. Seifert, R. Schmidt, *Phys. Rev. Lett.* **1996**, *76*, 3289 – 3292.

[45] A. Kaiser, C. Leidlmair, P. Bartl, S. Zöttl, S. Denifl, A. Mauracher, M. Probst, P. Scheier, O. Echt, *J. Chem. Phys.* **2013**, *138*, 074311.

[46] S. Prasalovich, K. Hansen, M. Kjellberg, V. N. Popok, E. E. B. Campbell, *J. Chem. Phys.* **2005**, *123*, 084317.

[47] C. E. Klots, *Z. Phys. D* **1991**, *21*, 335 – 342; R. Casero, J. M. Soler, *J. Chem. Phys.* **1991**, *95*, 2927 – 2935; K. Hansen, U. Näher, *Phys. Rev. A* **1999**, *60*, 1240 – 1250.

[48] L. An der Lan, P. Bartl, C. Leidlmair, R. Jochum, S. Denifl, O. Echt, P. Scheier, *Chem. Eur. J.* **2012**, *18*, 4411 – 4418.

[49] It is not possible to use the method of running averages[46] near the ends of the data set. Therefore, for $n < 10$ a smooth function was obtained by fitting a polynomial of third order to the size range $1 < n < 10$.

[50] The binding energy $-E$ differs from the dissociation energy D_n as defined in Equation (1). It would be computationally costly to determine D_n because simulations would have to be run for all values of n if one wants to see the energy difference for first shells, dimple sites, and so on. Nevertheless, the binding and dissociation energies are expected to be strongly correlated.

[51] Occasionally, the initial configurations used in the simulations led to minor variations in the distributions.

[52] R. Ditchfield, W. J. Hehre, J. A. Pople, *J. Chem. Phys.* **1971**, *54*, 724.

[53] F. Tournus, J. C. Charlier, P. Melinon, *J. Chem. Phys.* **2005**, *122*, 094315.

[54] H. Zettergren, Y. Wang, A. Lamsabhi, M. Alcami, F. Martin, *J. Chem. Phys.* **2009**, *130*, 224302.

[55] L. An der Lan, P. Bartl, C. Leidlmair, H. Schöbel, R. Jochum, S. Denifl, T. D. Märk, A. M. Ellis, P. Scheier, *J. Chem. Phys.* **2011**, *135*, 044309.

[56] S. Nosé, *Mol. Phys.* **1984**, *52*, 255 – 268; W. G. Hoover, *Phys. Rev. A* **1985**, *31*, 1695 – 1697.

[57] S. Grimme, *J. Comput. Chem.* **2006**, *27*, 1787 – 1799; J.-D. Chai, M. Head-Gordon, *Phys. Chem. Chem. Phys.* **2008**, *10*, 6615 – 6620.

[58] P. Hobza, *Annu. Rep. Prog. Chem. Sect. C* **2011**, *107*, 148 – 168; J. Klimeš, A. Michaelides, *J. Chem. Phys.* **2012**, *137*, 120901; M. P. Waller, H. Kruse, C. Muck-Lichtenfeld, S. Grimme, *Chem. Soc. Rev.* **2012**, *41*, 3119 – 3128; S. E. Huber, S. Dalnodar, W. Kausch, S. Kimeswenger, M. Probst, *AIP Adv.* **2012**, *2*, 032180.

[59] G. E. Scuseria, C. L. Janssen, H. F. Schäfer III., *J. Chem. Phys.* **1988**, *89*, 7382 – 7387.

[60] T. H. Dunning, *J. Chem. Phys.* **1989**, *90*, 1007 – 1023.

[61] W. J. Hehre, R. Ditchfield, J. A. Pople, *J. Chem. Phys.* **1972**, *56*, 2257 – 2261.

[62] P. C. Hariharan, J. A. Pople, *Theor. Chim. Acta* **1973**, *28*, 213 – 222.

[63] Gaussian 09, Revision A.02, M. J. Frisch, G. W. Trucks, H. B. Schlegel, G. E. Scuseria, M. A. Robb, J. R. Cheeseman, G. Scalmani, V. Barone, B. Mennucci, G. A. Petersson, H. Nakatsuji, M. Caricato, X. Li, H. P. Hratchian, A. F. Izmaylov, J. Bloino, G. Zheng, J. L. Sonnenberg, M. Hada, M. Ehara, K. Toyota, R. Fukuda, J. Hasegawa, M. Ishida, T. Nakajima, Y. Honda, O. Kitao, H. Nakai, T. Vreven, J. A. Montgomery, Jr., J. E. Peralta, F. Ogliaro, M. Bearpark, J. J. Heyd, E. Brothers, K. N. Kudin, V. N. Staroverov, R. Kobayashi, J. Normand, K. Raghavachari, A. Rendell, J. C. Burant, S. S. Iyengar, J. Tomasi, M. Cossi, N. Rega, J. M. Millam, M. Klene, J. E. Knox, J. B. Cross, V. Bakken, C. Adamo, J. Jaramillo, R. Gomperts, R. E. Stratmann, O. Yazyev, A. J. Austin, R. Cammi, C. Pomelli, J. W. Ochterski, R. L. Martin, K. Morokuma, V. G. Zakrzewski, G. A. Voth, P. Salvador, J. J. Dannenberg, S. Dapprich, A. D. Daniels, Ö. Farkas, J. B. Foresman, J. V. Ortiz, J. Cioslowski, D. J. Fox, Gaussian, Inc., Wallingford CT, **2009**.

[64] I. T. Todorov, W. Smith, K. Trachenko, M. T. Dove, *J. Mater. Chem.* **2006**, *16*, 1911 – 1918.